Nano-Structures & Nano-Objects 2 (2015) 28–34

Contents lists available at ScienceDirect

Nano-Structures & Nano-Objects

journal homepage: www.elsevier.com/locate/nanoso

Synthesis of ruthenium@graphene nanomaterials in propylene carbonate as re-usable catalysts for the solvent-free hydrogenation of benzene

Raquel Marcos Esteban [a], Kai Schütte [a], Dorothea Marquardt [a], Juri Barthel [b], Fabian Beckert [c], Rolf Mülhaupt [c,d], Christoph Janiak [a,*]

[a] Institut für Anorganische Chemie und Strukturchemie, Heinrich Heine Universität Düsseldorf, 40204 Düsseldorf, Germany

[b] Ernst Ruska-Centre for Microscopy and Spectroscopy, Forschungszentrum Jülich GmbH and RWTH Aachen University, 52425 Jülich, Germany

[c] Freiburger Material-forschungszentrum (FMF) and Institut für Makromolekulare Chemie, Universität Freiburg, Stefan-Meier-Str. 21-31, 79104 Freiburg, Germany

[d] FRIAS, Freiburg Institute for Advanced Studies, Albertstr. 19, 79104, Freiburg, Germany

HIGHLIGHTS

- Deposition of ruthenium nanoparticles (Ru-NPs) on graphene material.
- Propylene carbonate as non-toxic and biodegradable solvent for the synthesis of Ru-NPs.
- Quick and easy method for the preparation of Ru-NPs by microwave irradiation.
- Synthesis of stable, small (∼4 nm diameter) and catalytic active Ru-NPs.
- Hydrogenation catalysis of benzene under solvent-free conditions.

GRAPHICAL ABSTRACT

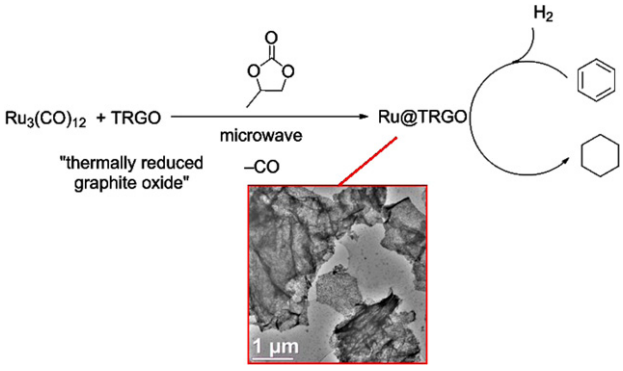

ARTICLE INFO

Article history:
Received 1 June 2015
Received in revised form
16 July 2015
Accepted 20 July 2015

Dedicated to Prof. Ekkehard Hahn on the occasion of his 60th birthday

Keywords:
Ruthenium nanoparticles
Graphene
Thermally reduced graphite oxide, TRGO
Benzene hydrogenation
Catalysis

ABSTRACT

Ruthenium nanoparticles (Ru-NPs) can be deposited on thermally reduced graphite oxide (TRGO) in propylene carbonate (PC). Propylene carbonate is a biodegradable and non-toxic solvent. Synthesis of Ru-NPs and deposition on TRGO were achieved by decomposition of ruthenium dodecacarbonyl, $Ru_3(CO)_{12}$, by microwave irradiation. Ru@graphene nanomaterials were identified and characterized by high resolution transmission electron microscopy (TEM, HR-TEM), energy-dispersive X-ray diffraction (EDX), selected area electron diffraction (SAED), X-ray photoelectron spectroscopy (XPS) and powder X-ray diffraction (PXRD) with a small diameter and size distribution of 7 ± 4 nm Ru-NPs on TRGO. These Ru@graphene nanomaterials are active catalysts for the solvent-free hydrogenation of benzene to cyclohexane under mild conditions (100 °C, 10 bar) with activities of 34,000 (mol cyclohexane) · (mol Ru)$^{-1}$ · h^{-1} and over 90% conversion in at least ten consecutive runs.

* Corresponding author. Tel.: +49 211 81 12286; fax: +49 211 81 12287.
E-mail address: janiak@uni-duesseldorf.de (C. Janiak).

http://dx.doi.org/10.1016/j.nanoso.2015.07.002

1. Introduction

Properties of the transition metal nanoparticles (M-NPs) are of general interest due to their various applications in science and technology [1–3]. The small size together with a large surface area of M-NPs offers a wide range of opportunities in the field of catalysis [4–8].

Ruthenium is an attractive catalytic metal because of its lower economical price compared to other noble metals such as palladium or rhodium. The selectivity of Ru-NP catalysts for the hydrogenation of C=C carbon double bonds in alkenes or arenes [9–12] allows for their possible application in hydrogenation processes such as the relevant hydrogenation of benzene or cyclohexene to cyclohexane [13], or in the Fischer–Tropsch synthesis [14,15] for the production of hydrocarbons.

Synthesis of ruthenium nanoparticles [4] is possible by simple reduction of common salts, $RuCl_3$ [16,17], or by decomposition of zero-valent compounds, such as $Ru_3(CO)_{12}$ [18–20] or [Ru(cyclooctadiene)(cyclooctatetraene)] [21–25].

For small M-NPs agglomeration and aggregation due to the Ostwald ripening [26,27] needs to be prevented and a stabilizing ligand shell is often needed. Such stabilizers can be organic donor ligands or polymers, [5,22,28–30] or ionic liquids, [31–35] which form a protective layer (shell) around the particles (core). Also immobilization or deposition of nanoparticles on supports such as graphene [36–39], carbon nanotubes [40,41] or more often Al_2O_3 [13] is a means to prevent agglomeration.

Over the last years, thermally reduced graphite oxide [42–48] also simply called "graphene", has been rediscovered as an extremely versatile carbon material [49–51]. Because of the functional groups present in TRGO (Fig. S1 in Supporting Information), the sorption of ions and molecules is possible [49]. This and the high specific surface area of TRGO of 400 $m^2\ g^{-1}$ up to 1500 $m^2\ g^{-1}$, make them promising materials for catalytic applications [49]. Metal-nanoparticles on carbon materials are of recent interest [52–60].

Organic carbonates (Fig. 1) are used in industry for degreasing, gas treating or cleaning [62]. Organic carbonates are polar solvents with a wide range of liquid temperature range (for propylene carbonate, PC mp −49 °C, bp 243 °C), and with a low flammability, low volatility and low (eco)toxicity [61]. Biodegradable PC is used as solvent in the FLUOR process for CO_2 removal [63,64], in the research on lithium-ion batteries [65–67] or as co-solvent for cosmetics due to its low toxicity and irritability [68,69].

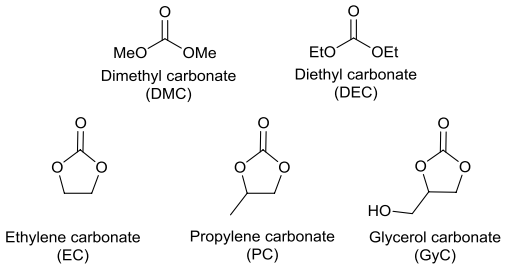

Fig. 1. Selected organic carbonates: dimethyl carbonate (DMC); diethyl carbonate (DEC); ethylene carbonate (EC); propylene carbonate (PC); glycerol carbonate (GyC) [61].

There appear to be only few reports on metal nanoparticle synthesis in organic carbonates in the literature [70–73]. The role of propylene carbonate is not fully clear yet. Its carbonate oxygen functionality may coordinate to the metal surface and thereby play the role of a capping agent. Only recently a more comprehensive report on the synthesis of Mo-, W-, Re-, Fe-, Ru-, Os-, Co-, Rh-, or Ir-metal-nanoparticles in propylene carbonate has appeared. These M-NPs were obtained (without TRGO support) from their metal carbonyls by means of microwave irradiation as small particles with narrow diameter distributions (*e.g.*, for Ru-NPs 2.7 ± 0.5 nm from $Ru_3(CO)_{12}$ or for Os-NPs 3.0 ± 1.5 nm from $Os_3(CO)_{12}$) [20]. When 3-mercaptopropionic acid, HS-$(CH_2)_2$-COOH was added post-synthetically to this Ru-NP/PC dispersion, the isolated ligand-capped nanoparticles were significantly larger (13 (±4) nm diameter). Thus, the introduction of a protic organic thiol ligand more than doubles the size of the resulting capped metal nanoparticles. Therefore, the thiol ligand addition must perturb and weaken the stabilizing property of propylene carbonate towards the M-NPs so that further M-NP agglomeration is driven by the surface–surface interactions [20]. Cu-, Zn- and Cu/Zn nanobrass alloy nanoparticles were also obtained in PC without the use of extra-stabilizers and dispersions seemed to be stable up to six months [74]. The M-NP/PC dispersions have been tested for the hydrogenation of cyclohexene for Rh-NPs under mild conditions (4–10 bar H_2, 25–90 °C), to give turnover frequencies up to 1875 mol h^{-1} [20].

Here we report the deposition of Ru-NPs on thermally reduced graphite oxide (TRGO) by decomposition of $Ru_3(CO)_{12}$ in PC, and the use of the Ru@TRGO composite as catalyst for the hydrogenation of benzene.

2. Results and discussion

2.1. TRGO-supported Ru-NPs in propylene carbonate

Deposition of Ru-NPs on graphene (TRGO) can be achieved from the corresponding metal carbonyl, $Ru_3(CO)_{12}$, by the rapid and saving-energy method of microwave irradiation (MWI, 250 °C, 50 W, 10 min) with TRGO in propylene carbonate (PC) (Scheme 1).

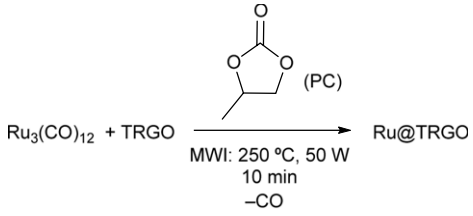

Scheme 1. Synthesis of Ru@TRGO nanomaterials by means of decomposition from $Ru_3(CO)_{12}$ in the presence of TRGO using the energy input of microwave irradiation.

TRGO as support can allow for the synthesis (nucleation and growth) and stabilization of metal nanoparticles because of the functional groups on its surface, where the metal nanoparticles adsorb (bind) and consequently their agglomeration is limited [49,51].

Decomposition of $Ru_3(CO)_{12}$ was followed by infrared spectroscopy (IR) and no bands for the carbonyl bonds at 2020 and 2060 cm^{-1} were found after MWI, indicating full conversion of the metal carbonyl precursor to Ru-NPs (Fig. S3). Of course, our spectroscopic measurement was not sensitive enough to rule out some CO coordination to the surface of the formed Ru nanoparticles.

The resulting Ru@TRGO nanomaterials were characterized by powder X-ray diffraction (PXRD) (Fig. 2). The characteristic reflections at 2θ values of 38.1°, 42.2°, 43.7°, 58.3°, 69.1°, 78.3°, 82.4°, 84.5°, and 86.1° correspond to the indicated [010], [002], [011], [012], [110], [013], [020], [122], and [021] reflections, respectively, of bulk ruthenium metal (Fig. 2). Reflections in the 2θ region between 5 and 25° are derived from TRGO (see Fig. S2 in Supp. Info). The average diameter of the Ru-NPs was calculated by the Debye–Scherrer equation to 10.5 nm from the half-width of the [010] reflection. Characterization of the Ru@TRGO nanomaterials

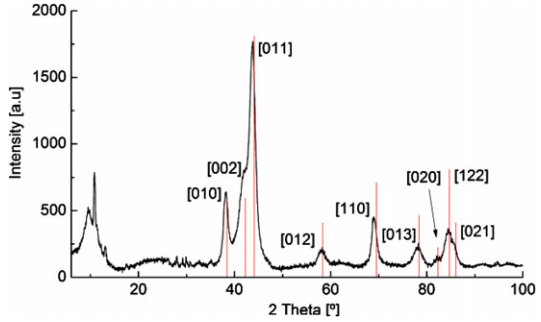

Fig. 2. PXRD of Ru-NPs deposited on TRGO after decomposition by means of microwave irradiation in comparison with the literature (Crystallographic open database COD. 9008513, red bars). Reflections between 5 and 25° are due to TRGO (cf. Fig. S2 in Supp. Info.). (For interpretation of the references to colour in this figure legend, the reader is referred to the web version of this article.)

by transmission electron microscopy (TEM) (Fig. 3) and high-resolution transmission electron microscopy (HR-TEM) with selected area electron diffraction (SAED) (Fig. 4) yielded a diameter and distribution of 7 ± 4 nm for the Ru-NPs (see TEMs with histograms in Fig. S4) and illustrated the nanocrystalline nature. High-resolution TEM images in Fig. 3 (at 10 nm) and Fig. 4 (at 2 nm) showed facetted Ru nanoparticles of presumably cuboctahedral nature. The shape of a crystalline cuboctahedron most closely approaches those of a sphere. From interference of the electron beam with the Ru atoms the highly crystalline, symmetrical most likely cuboctahedral structure of the Ru nanoparticles became visible in the form of their lattice planes (Fig. 4). Energy-dispersive X-ray spectroscopy (EDX) (Fig. S5) only gave the expected bands for Ru metal (Ru-Kα, -Lα1, -Lβ1, -Lγ1, -Mα, -Mγ) besides the bands for carbon and copper of the TRGO and the carbon-coated copper grid.

X-ray photoelectron spectroscopy (XPS) measurements yielded composition of the Ru@TRGO nanomaterials (Fig. 5 and Fig. S6). A content of 3.5 wt% Ru was calculated based on the peaks at 460.9 eV (Ru $3p_{3/2}$) and at 283.4 eV (C 1s). A zero-valent oxidation state of ruthenium is verified from the peak at 279.4 eV, which corresponds to Ru $3d_{5/2}$ [75]. The C 1s and O 1s peak at 283.4 and 530.9 eV, respectively, are associated to graphene and its functional oxygen groups. The O 1s band corresponds to C=O and O=C–OH groups [76].

2.2. Hydrogenation of benzene

Ru@TRGO was tested as heterogeneous catalyst for the hydrogenation of benzene to cyclohexane (Scheme 2).

In a typical hydrogenation reaction Ru@TRGO (5.0 mg, containing 3.5 wt% Ru, 1.73×10^{-3} mmol), and the substrate (benzene, 1.0 mL, 11.14 mmol) were loaded in a stainless-steel autoclave, equipped with a glass inlay to avoid any interference from the steel surface. The autoclave was purged with H_2 at least three times and

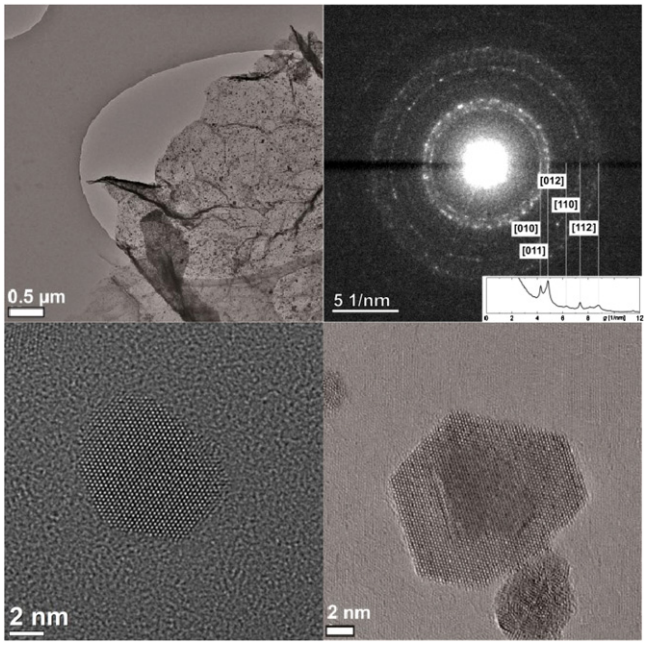

Fig. 4. HR-TEM and electron diffraction of Ru@TRGO synthesized in propylene carbonate. The upper row shows a TRGO flake with many Ru nanoparticles attached, and an electron diffraction pattern taken from this area. The inset diagram shows the average diffraction intensity depending on spatial frequencies in the diffraction pattern. The lower row displays two high-resolution TEM images of single Ru nanoparticles revealing their nano-crystalline and presumably cuboctahedral nature.

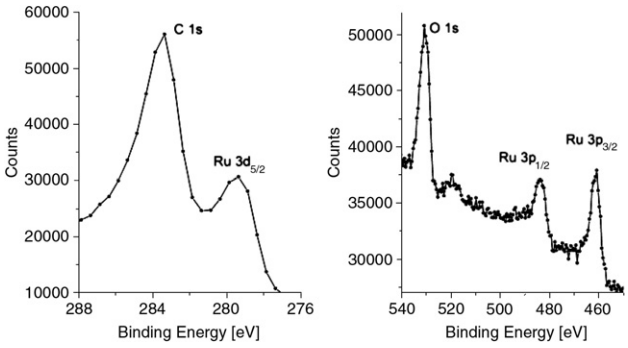

Fig. 5. Enlarged regions of the XPS spectrum (see Fig. S6 in Supp. Info. for full spectrum) of Ru@TRGO nanomaterial with a calculated 3.5 wt% loading of Ru on TRGO.

pre-heated to 100 °C. Once the desired temperature was reached the autoclave was pressurized to 10 bars of H_2 and the reaction mixture stirred (800 rpm) for 20 min. After this time the autoclave was cooled down and the substrate/product mixture was

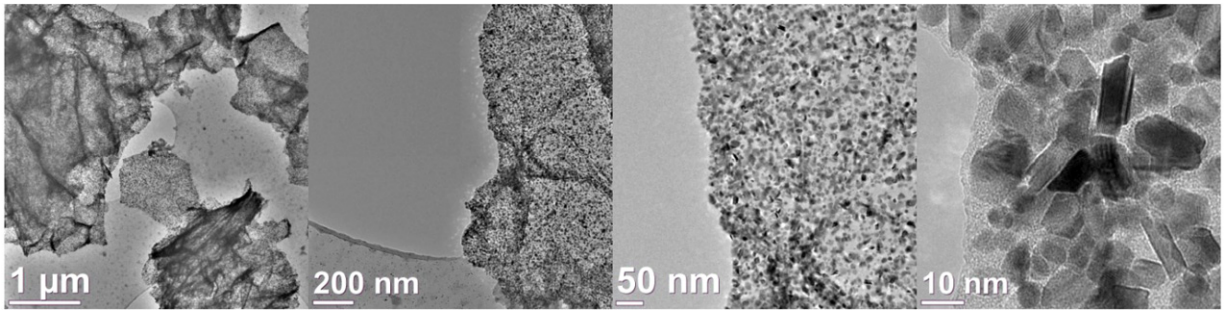

Fig. 3. TEM images of Ru@TRGO nanomaterials synthesized in propylene carbonate.

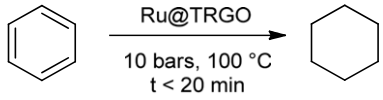

Scheme 2. Hydrogenation of benzene to cyclohexane with Ru@TRGO nanocomposites under solvent-free conditions.

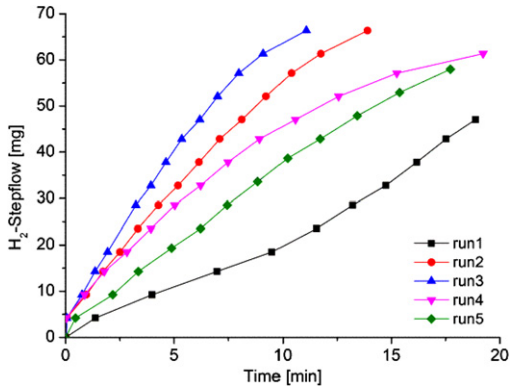

Fig. 6. H_2-uptake over time for the hydrogenation of benzene (0.87 g, 1.0 mL, 11.14 mmol) with Ru@TRGO (5.0 mg, containing 3.5 wt% Ru, 1.73×10^{-3} mmol) at a benzene/metal ratio of 6436, 100 °C and 10 bars H_2. A 100% conversion corresponds to an H_2-uptake of 67.4 mg (33.4 mmol, 802 mL). For clarity the runs 6–10 are given in Fig. S7 in the Supporting Information.

condensed under vacuum into a cold trap. The H_2 uptake was monitored over time by a Büchi bpc press-flow controller (Fig. 6 and Fig. S7).

Conversion of benzene to cyclohexane was calculated based on the consumption of H_2 (Fig. 6 and Fig. S7). Additional measurements by gas chromatography, GC, show no formation of other products such as cyclohexene. The catalyst Ru@TRGO remained in the autoclave and could be re-used at least 10 times without significant loss of activity.

The Ru@TRGO catalyst increased its activity up to the third run to reach a turnover frequency (TOF) of ~34,330 (molcyclohexane) · (mol Ru)$^{-1}$ · h^{-1} (Table 1) near quantitative conversion in about 11 min (Fig. 6). Afterwards, the conversion decreased to 92.3% to stay constant between run 6 to 10 with activities (TOF) around 22,000 (mol cyclohexane) · (mol Ru)$^{-1}$ · h^{-1}.

Heterogeneous catalytic reactions are extremely complex and defects, the surface topology, and surface atom sites (edges, corners, steps) rather than the sole amount of surface atoms strongly influence the catalytic activity. We therefore suggest that the activity increase upon recycling is due to surface reconstruction creating more and more active sites. Increase in activity could also result from surface cleaning of adsorbed and deactivating solvent, carbon or oxygen species. Because of the TRGO support also further exfoliation could occur which would expose more Ru-NPs. The TOF calculation was based on the total quantity of Ru present in the nanomaterial. We note that only surface atoms and among them only a fraction will be catalytically active. If less than 5% of the metal atoms of the Ru-NPs are active surface sites then the activity would be more than 20-times higher on a per-active-metal-atom basis.

Graphene-supported metal nanoparticles were already investigated in our group for Ru- and Rh-NPs and synthesized in the ionic liquid (IL) 1-butyl-3-methylimidazolium tetrafluoroborate [36]. Lower activities were found for Ru- and Rh-NP@graphene in IL than here in propylene carbonate (Table 2). Apparently the remaining IL coating around the nanoparticles presents a diffusion barrier for the substrate species (benzene and H_2). Using M@TRGO/IL (M=Ru or Rh) at 50 or 75 °C with 4 bar of H_2 the time to achieve a

Table 1
Hydrogenation of benzene to cyclohexane with Ru@TRGO nanomaterials[a].

Run	Conversion (%)[b]	Time (min)[c]	TOF (h^{-1})[d]	TON[e]
1	69.8	18.9	14282	4494
2	98.5	13.9	27366	6340
3	98.5	11.1	34331	6340
4	91.0	19.2	18279	5858
5	86.0	17.7	18749	5537
6	92.3	16.9	21059	5939
7	92.3	15.9	22367	5939
8	92.3	16.2	22035	5939
9	92.3	15.7	22767	5939
10	84.4	11.2	29286	5457

[a] Hydrogenation reaction at 100 °C, 10 bars H_2 using Ru@TRGO (mol benzene/mol Ru = 6436).
[b] Calculated based on the H_2-consumption.
[c] Time needed for the given maximum conversion.
[d] Turnover frequency = activity as (mol cyclohexane) · (mol Ru)$^{-1}$ · h^{-1}; with total quantity of Ru present in the nanomaterial.
[e] Turnover number as (mol cyclohexane) · (mol Ru)$^{-1}$.

conversion near 98% was almost four hours (even when cyclohexene was used instead of benzene). The reason to run the catalysis in this work at 100 °C and 10 bar of H_2 was the desire to achieve a conversion of 80%–90% in less than 30 min. Although not tested here, we can assume that the Ru@TRGO/PC system will also be active under milder conditions.

Table 2
Metal@graphene nanomaterials as catalyst for the hydrogenation reaction of benzene[a] or cyclohexene[b] to cyclohexane.

M-NPs/Solvent[c]	pH_2 (bar)	T (°C)	Time[d] (h)	TOF[e] (h^{-1})	Ref.
Ru@TRGO/PC	10	100	<0.33	34330[a]	This work
Ru@TRGO/IL	4	75	4	1570[b]	[37]
Rh@TRGO/IL	4	50	4	310[a]	

[a] Hydrogenation of benzene or.
[b] cyclohexene to cyclohexane.
[c] PC = propylene carbonate or IL = 1-butyl-3-methyltetrafluoroborate [BMIm][BF_4].
[d] For near quantitative conversion.
[e] Turnover frequency as (mol cyclohexane) · (mol metal)$^{-1}$ · h^{-1}.

A wide range of supports for the immobilization of Ru-NPs has been tested for the hydrogenation of benzene (Table 3). Dupont et al. recently reported the deposition of Ru-NPs on modified Al_2O_3 supports with anchored imidazolium-ILs achieving a TOF of 9180 h^{-1} for the hydrogenation of benzene to cyclohexene [13]. Carbon-based supports are also suitable for the stabilization of Ru-NPs and their application in catalysis, Ru-NPs deposited on carbon nanotubes [40] show activities up to ~6900 h^{-1}, and activities around ~35,000 h^{-1} were found for embedded ruthenium nanoparticles on ordered mesoporous carbon [77].

After ten consecutive hydrogenation runs the Ru@TRGO catalyst was analyzed by TEM and SAED (Fig. 7). The nanoparticles retained their crystallinity as is evident from their facets in the TEM and the reflections in the SAED. The average diameters of the Ru-NPs essentially did not change with now 7.2 ± 3.4 nm (for histogram and EDX see Fig. S8 in Supp. Info.).

Concerning leaching we note that even in solution or dispersion, that is, without the TRGO support, the Ru-NP will be catalytically active. This was shown by their use as hydrogenations catalysts for cyclohexene as Ru-nanoparticle/IL dispersion [18]. A leaching process would not have led to removal from the catalyst dispersion here as we removed the products and starting materials by evaporation under vacuum so that no catalyst part could be removed.

Table 3
Hydrogenation reaction for benzene with supported Ru-NPs.

Catalyst[a]	H_2 pressure (bar)	T (°C)	TOF[b] (h^{-1})	Ref.
Ru/HEA-16-Cl	30	20	600[c]	[7,78]
Ru/MMT	8	110	4000	[79]
Ru/CNTs	4	80	6983	[40]
Ru/SiO_2	20	100	5000	[80]
Ru/IL-Al_2O_3	4	75	9180[d]	[77]
Ru-OMC	4	110	35,112	[77]

[a] HEA-16-Cl = *N*,*N*-dimethyl-N-cetyl-N-(2-hydroxyethyl)ammonium chloride, MMT = montmorillonite, CNT = carbon nanotubes, IL = ionic liquid, OMC = ordered mesoporous ruthenium containing carbon.
[b] Turnover frequency = activity as (mol cyclohexane) · (mol total Ru)$^{-1}$ h^{-1} unless noted otherwise.
[c] TOF as (mol consumed H_2) · (mol total Ru)$^{-1}$ h^{-1}.
[d] TOF as (mol benzene conversion) · (mol surface Ru)$^{-1}$ h^{-1}.

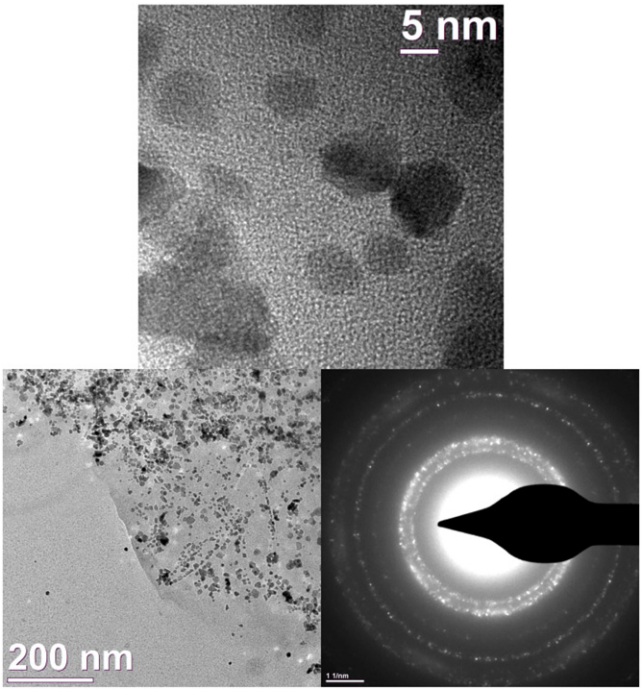

Fig. 7. TEM and SAED of Ru@TRGO after ten consecutive runs in the hydrogenation of benzene to cyclohexane. The black line corresponds to the beam stopper. (For more HR-TEM images see Fig. S9 in Supp. Info.)

3. Conclusion

We describe a straightforward method for the deposition of ruthenium nanoparticles (Ru-NPs) on thermally reduced graphite oxide (TRGO) using propylene carbonate as solvent. The formed Ru-NPs have a size distribution of 7 ± 4 nm and no extra capping ligand or stabilizer is needed for their immobilization and stabilization.

The Ru@TRGO nanomaterials show higher catalytic activities for the hydrogenation of benzene in comparison with their Rh- or Ir-@TRGO analogs, which were synthesized in ionic liquids instead of in organic carbonates. Propylene carbonate, PC, can readily and more completely be removed from the Ru@TRGO composite so as to avoid a diffusion barrier which is otherwise given by a remaining IL layer around the nanoparticles. As a consequence the Ru@TRGO catalysts achieve near quantitative conversion in less than 20 min with turnover frequencies over 18,000 and up to 34,000 (mol cyclohexane) · (mol Ru)$^{-1}$ · h^{-1} for at least 10 consecutive runs under solvent-free conditions. Ru@TRGO nanomaterials exhibit also higher activities than other reported immobilized Ru-NPs.

4. Experimental section

4.1. Materials and methods

All experiments were done using Schlenk techniques under inert atmosphere. Triruthenium dodecacarbonyl $Ru_3(CO)_{12}$ (99% purity) was purchased from ABCR chemicals and thermally reduced graphene oxide (TRGO) was prepared in a two steps oxidation/thermal reduction process using natural graphite (type KFL 99.5 from AMG Mining AG, former Kropfmühl AG, Passau, Germany) as raw material. The graphite oxidation process of Hummers and Offeman [81] was employed. Benzene was purchased by VWR (p.A.), dried with sodium, distilled and stored over 4 Å molecular sieve.

Propylene carbonate was dried under vacuum at 100 °C (10^{-3} mbar) for at least three days. IR spectra were measured on a Bruker TENSOR 37 IR spectrometer in the range from 4000 to 500 cm^{-1} as KBr disks.

The X-ray photoelectron spectroscopy, XPS- (ESCA-) measurement was performed with a Fisons/VG Scientific ESCALAB 200X xp-spectrometer, operating at room temperature, a pressure of $1.0 \cdot 10^{-8}$ bar and a sample angle of 30°. Photoelectron spectra were recorded using polychromatic Al-K_α excitation (14 kV, 20 mA) and an emission angle of 0°. Calibration of the XPS was carried out by recording spectra, using Al K_α X-rays, from clean samples of copper, silver and gold, at 20 eV and 10 eV pass energies and comparison with reference values.

TEM micrographs were recorded with an FEI Tecnai g2 f20 operated at 200 kV accelerating voltage. High-resolution TEM images were recorded with an FEI Titan 80–300 image CS-corrected electron microscope at an accelerating voltage of 300 kV. Samples were prepared using 200 μm carbon-coated copper grids. The size distribution was determined manually and using Gatan Digital Micrograph for at least 150 nanoparticles. For the automatic selection of the nanoparticles we introduced a threshold in the picture, where the nanoparticles will have a different intensity as the background. Noteworthy the automatic determination gave a smaller average diameter than the manual measurement.

High angle energy dispersive X-ray (EDX) detector with a resolution of 136 eV or better for Mn K-alpha radiation, the exposure time for individual EDX spectra was 3 min.

4.2. Synthesis of Ru@TRGO nanomaterials in propylene carbonate

$Ru_3(CO)_{12}$ (25.4 mg, 3.97×10^{-3} mmol) together with 4.7 mg of TRGO (0.2 wt% related to 2.41 g of PC) were dispersed and sonicated for 6 h at 30 °C in PC (2 mL, 2.41 g).

Metal carbonyl decomposition was done by means of microwave irradiation (CEM Discover) at 250 °C, 50 W, 4 bar and 10 min. The volatiles (CO) were removed under vacuum and the black dispersion washed with distilled water (5 × 6 mL) and centrifuged. Finally the Ru@TRGO nanomaterials were dried under vacuum at 100 °C for several hours.

4.3. Hydrogenation of benzene to cyclohexane

All catalytic processes were done using stainless-steel autoclaves under inert atmosphere. Each autoclave was equipped with a glass inlay to avoid any effect of the steel in the reaction.

The desired amount of catalyst (Ru@TRGO, 5 mg containing 3.5% Ru, 1.73×10^{-3} mmol Ru) together with the substrate (benzene, 1 mL, 0.87 g, 11.14 mmol) were loaded in the autoclave. The autoclave was purged three times with H_2 and heated to 100 °C. Once the set temperature was achieved, the autoclave was charged with 10 bars of H_2 and the reaction mixture was stirred (800 rpm) for 20 min. After this time the autoclave was cooled down and

depressurized. The organic volatile were isolated by evaporation and condensation under vacuum in a cold trap. The products were analyzed by GC and conversion was calculated in relation to the H_2 consumption.

Conversion of benzene to cyclohexane was determined by gas chromatography (GC) (Perkin Elmer 8500 HSB 6, equipped with a DB-5 film capillary column, 60 m × 0.32 mm, film thickness 25 μm, oven temperature 40 °C, N2 carrier flow 120 L/min and a flame ionization detector (FID), 250 °C detector temperature). The samples were analyzed by putting a drop of the product into a GC sample vial together with 1 mL of distilled water.

H_2-uptake measurements were followed with a Büchi bpc pressflow controller.

The catalyst could be recovered and re-used for at least 10 times. All procedures were repeated at least twice to evaluate the reproducibility of the process.

Acknowledgment

Authors are thankful to the Deutsche Forschungsgemeinschaft (DFG) for grant Ja466/31-1 within priority program SPP 1708.

Appendix A. Supplementary data

Supplementary material (PXRD pattern of TRGO-400, IR of Ru@TRGO, diameter distribution histogram, EDX-spectrum, full XPS, all H_2-stepflow curves in benzene hydrogenation and additional TEM micrographs) related to this article can be found online at http://dx.doi.org/10.1016/j.nanoso.2015.07.002.

References

[1] J.A. Dahl, B.L.S. Maddux, J.E. Hutchison, Chem. Rev. 107 (2007) 2228–2269.
[2] K. Saha, S.S. Agasti, C. Kim, X. Li, V.M. Rotello, Chem. Rev. 112 (2012) 2739–2779.
[3] H. Goesmann, C. Feldmann, Angew. Chem. Int. Ed. 49 (2010) 1362–1395.
[4] A. Roucoux, J. Schluz, H. Patin, Chem. Rev. 102 (2002) 3757–3778.
[5] D. Astruc, F. Lu, J.R. Aranzaes, Angew. Chem. Int. Ed. 44 (2005) 7852–7872.
[6] D. Wang, Y. Li, Adv. Mater. 23 (2011) 1044–1060.
[7] D. Astruc, Nanoparticles and Catalysis, Wiley-VCH, Weinheim, 2007.
[8] J.D. Scholten, B.C. Leal, J. Dupont, ACS Catal. 2 (2012) 184–200.
[9] T. Naota, H. Takaya, S.-I. Murahashi, Chem. Rev. 98 (1998) 2599–2660.
[10] A. Gual, C. Godard, S. Castillón, C. Claver, Dalton Trans. 39 (2010) 11499–11512.
[11] Y. Huang, Y. Mao, Y. Cheng, L. Wang, X. Li, Appl. Catal. A: General 495 (2015) 124–130.
[12] J. Aguilera, I. Favier, M. Sans, A. Mor, A. Álvarez-Larena, O. Illa, M. Gómez, R.M. Ortuño, Eur. J. Org. Chem. 4 (2015) 810–819.
[13] L. Foppa, L. Luza, A. Gua, D.E. Weibel, D. Eberhardt, S.R. Texeira, J. Dupont, Dalton Trans. 44 (2015) 2827–2834.
[14] V.R.R. Pendyala, W.D. Shafer, G. Jacobs, U.M. Graham, S. Khalid, B.H. Davis, Catal. Lett. 145 (2015) 893–904.
[15] A. Haghtalab, A. Mosayebi, Int. J. Hydrog. Energy 39 (2014) 18882–18893.
[16] G. Viau, R. Brayner, L. Poul, N. Chakroune, E. Lacze, F. Fiévet-Vicent, F. Fiévet, Chem. Mater. 15 (2003) 486–494.
[17] N. Chakroune, G. Viaiu, S. Ammar, L. Poul, D. Veautier, M.M. Chehimi, C. Mangeney, F. Villain, F. Fiévet, Langmuir 21 (2005) 6788–6796.
[18] C. Vollmer, E. Redel, K. Abu-Shandi, R. Thomann, H. Manyar, H. Hardacre, C. Janiak, Chem. Eur. J. 16 (2010) 3849–3858.
[19] C. Vollmer, C. Janiak, Coord. Chem. Rev. 255 (2011) 2039–2057.
[20] C. Vollmer, R. Thomann, C. Janiak, Dalton Trans. 41 (2012) 9722–9727.
[21] K. Pelzer, O. Vidoni, K. Philippot, B. Chaudret, V. Collière, Adv. Funct. Mater. 13 (2003) 118–126.
[22] C. Pan, K. Pelzer, K. Philippot, B. Chaudret, F. Dassenoy, P. Lecante, M.-J. Casanove, J. Am. Chem. Soc. 123 (2001) 7584–7593.
[23] T. Gutel, J. Garcia-Anton, K. Pelzer, K. Philippot, C.C. Santini, Y. Chauvin, B. Chaudret, J.-M. Basset, J. Mater. Chem. 17 (2007) 3290–3292.
[24] G. Salas, A. Podgorsek, P.S. Campbell, C.C. Santini, A.A.H. Pádua, M.F. Costa Gomes, K. Philippot, B. Chaudret, M. Turmine, Phys. Chem. Chem. Phys. 13 (2011) 13527–13536.
[25] E.T. Silveira, A.P. Umpierre, L.M. Rossi, G. Machado, J. Morais, G.V. Soares, I.J.R. Baumvol, S.R. Teixeira, R.F.P. Fichtner, J. Dupont, Chem. Eur. J. 10 (2004) 3734–3740.
[26] W. Ostwald, Z. Phys. Chem. 37 (1901) 385.
[27] W. Ostwald, Lehrbuch der Allgemeinen Chemie, Vol. 2, Part 1, Leipzig, Germany, 1896.
[28] H. Bönnemann, R.M. Richards, Eur. J. Inorg. Chem. 10 (2001) 2455–2480.
[29] L.D. Pachón, G. Rothenberg, Appl. Organomet. Chem. 22 (2008) 288–299.
[30] P. Graf, A. Mantion, A. Foelske, A. Shkilnyy, A. Măsić, A.F. Thünemann, A. Taubert, Chem. Eur. J. 15 (2009) 5831–5844.
[31] (a) C. Janiak, Z. Naturforsch. B 68 (2013) 1056–1089;
(b) K. Klauke, B. Hahn, K. Schütte, J. Barthel, C. Janiak, Nano-Struct. Nano-Objects 1 (2015) 24–31.
[32] C. Janiak, Metal nanoparticle synthesis in ionic liquids, in: J. Dupont, L. Kollar (Eds.), Ionic Liquids (ILs) in Organometallic Catalysis, in: Topics in Organometallic Chemistry, vol. 51, Springer, Heidelberg, 2015, pp. 17–53.
[33] C. Janiak, Metal nanoparticle synthesis in ionic liquids, in: C. Hardacre, V. Parvulescu (Eds.), Catalysis in Ionic Liquids: From Catalyst Synthesis to Application, RSC Publishing, Cambridge, 2014, pp. 537–577, Chapter 11.
[34] J. Dupont, J.D. Scholten, Chem. Soc. Rev. 39 (2010) 1780–1804.
[35] J. Dupont, J. Brazil, Chem. Soc. 15 (2004) 341–350.
[36] R. Fernandes, N. Patel, E. Edla, N. Bazzanella, D.C. Kothari, A. Miotello, Appl. Catal. A: General 495 (2015) 23–29.
[37] D. Marquardt, C. Vollmer, R. Thomann, P. Steurer, R. Mülhaupt, E. Redel, C. Janiak, Carbon 49 (2011) 1326–1332.
[38] C. Vollmer, M. Schröder, Y. Thomann, R. Thomann, C. Janiak, Appl. Catal. A: General 425–426 (2012) 178–183.
[39] N. Cao, W. Luo, G. Cheng, Int. J. Hydrog. Energy 38 (2013) 11964–11972.
[40] Y. Ma, Y. Huang, Y. Cheng, L. Wang, X. Li, Appl. Catal. A: General 484 (2014) 154–160.
[41] L. Wang, J. Chen, L. Ge, V. Rudolph, Z. Zhu, J. Phys. Chem. C. 117 (2013) 4141–4151.
[42] G.M. Scheuermann, L. Rumi, P. Steurer, W. Bannwarth, R. Mülhaupt, J. Am. Chem. Soc. 131 (2009) 8262–8270.
[43] S. Stankovich, D.A. Dikin, G.H.B. Dommett, K.M. Kohlhaas, E.J. Zimney, E.A. Stach, R.D. Piner, S.T. Nguyen, R.S. Ruoff, Nature 442 (2006) 282–286.
[44] A.K. Geim, K.S. Novoselov, Nature Mater. 6 (2007) 183–191.
[45] D. Li, R.B. Kaner, Science 320 (2008) 1170–1171.
[46] P. Steurer, R. Wissert, R. Thomann, R. Mülhaupt, Macromol. Rapid Commun. 30 (2009) 316–327.
[47] M.J. McAllister, J.L. Li, D.H. Adamson, H.C. Schniepp, A.A. Abdala, J. Liu, M. Herrera-Alonso, D.L. Milius, R. Car, R.K. Prud'homme, I.A. Aksay, Chem. Mater. 19 (2007) 4396–4404.
[48] H.C. Schniepp, J.L. Li, M.J. McAllister, H. Sai, M. Herrera-Alonso, D.H. Adamson, R.K. Prud'homme, R. Car, D.A. Saville, I.A. Aksay, J. Phys. Chem. B 110 (2006) 8535–8539.
[49] G. Goncalves, P.A.A.P. Marques, C.M. Granadeiro, H.I.S. Nogueira, M.K. Singh, J. Grácio, Chem. Mater. 21 (2009) 4796–4802.
[50] C.N.R. Rao, A.K. Sood, R. Voggu, K.S. Subrahmanyam, J. Phys. Chem. Lett. 1 (2010) 572–580.
[51] H.P. Boehm, E. Stumpp, Carbon 45 (2007) 1381–1383.
[52] H.B. Li, W.J. Kang, B.J. Xi, Y. Yan, H.Y. Bi, Y.C. Zuhu, Y.T. Qian, Carbon 48 (2010) 464–469.
[53] H. Park, J.S. Kim, B.G. Choi, S.M. Jo, D.Y. Kim, W.H. Hong, S.-Y. Jang, Carbon 48 (2010) 1325–1330.
[54] D.N. Ventura, R.A. Stone, K.S. Chen, H.H. Hariri, K.A. Riddle, T.J. Fellers, C.S. Yun, G.F. Strouse, H.W. Kroto, S.F.A. Acquah, Carbon 48 (2010) 987–994.
[55] S. Kudo, T. Maki, K. Miura, K. Mae, Carbon 48 (2010) 1186–1195.
[56] K. Scholz, J. Scholz, A.J. McQuilla, G. Wagner, O. Klepel, Carbon 48 (2010) 1788–1798.
[57] Y.H. Kim, Y.T. Kim, H. Kim, D. Lee, Carbon 48 (2010) 2072–2084.
[58] V. Tzitzios, V. Georgakilas, E. Oikonomou, M. Karakassides, D. Petridis, Carbon 44 (2006) 848–853.
[59] D. Marquardt, F. Beckert, F. Pennetreau, F. Tölle, R. Mülhaupt, O. Riant, S. Hermans, J. Barthel, C. Janiak, Carbon 66 (2014) 285–294.
[60] R. Marcos Esteban, K. Schütte, P. Brandt, H. Marquardt, D. Meyer, F. Beckert, R. Mülhaupt, H. Kölling, C. Janiak, Nano-Struct. Nano-Objects 1 (2015) http://dx.doi.org/10.1016/j.nanoso.2015.07.001.
[61] B. Schäffner, F. Schäffner, S.P. Verevkin, A. Börner, Chem. Rev. 110 (2010) 4554–4581.
[62] J.H. Clements, Ind. Eng. Chem. Res. 42 (2003) 663–674.
[63] J. Mak, D. Nielsen, D. Schulte, LRGCC Conf. Proc. 57 (2007) 267–280.
[64] A.L. Kohl, P.A. Buckingham, Oil Gas J. 58 (1960) 146.
[65] G.G. Eshetu, J.-P. Bertrand, A. Lecocq, S. Grugeon, S. Laurelle, M. Armand, G. Marlair, J. Power Sources 269 (2014) 804–811.
[66] R. Jasinski, J. Electroanal. Chem. 15 (1967) 89–91.
[67] K.K.D. Ehinon, S. Naille, R. Dedryvère, P.-E. Lippens, J.-C.Jumas D. Gonbeau, Chem. Mater. 20 (2008) 5388–5398.
[68] H. Cheng, R.R. Gadde, J. Pharm. Sci. 74 (1986) 695–696.
[69] A. Ansmann, B. Boutty, M. Dierker, Chem. Abstr. 149 (2008) 17219.
[70] M. Reetz, G. Lohmer, Chem. Commun. 16 (1996) 1921–1922.
[71] A. Behr, H. Schmidke, Chem. Ing. Tech. 65 (1993) 568–569.
[72] A. Behr, N. Döring, S. Durowicz-Heil, B. Ellenberg, C. Kozik, C. Lohr, H. Schmidke, Fat Sci. Technol. 95 (1993) 2–12.
[73] J. Demel, J. Čejka, S. Bakardjieva, P. Štěpnička, J. Mol. Catal. A 263 (2007) 259–265.
[74] K. Schütte, H. Meyer, C. Gemel, J. Barthel, R.A. Fischer, C. Janiak, Nanoscale 6 (2014) 3116–3126.
[75] J.F. Moulder, W.F. Stickle, P.E. Sobol, K.D. Bombem, Handbook of X-ray Photoelectron Spectroscopy: a Reference Book of Standard Spectra for Identification and Interpretation of XPS Data, 1992, Published by Physical Electronics Division.
[76] D. Yang, A. Velamakanni, G. Bozoklu, S. Park, M. Stoller, R.D. Piner, S. Stankovich, I. Jung, D.A. Field, C.A. Ventrice Jr., R.S. Ruoff, Carbon 47 (2009) 145–152.

[77] Y. Li, G. Lan, H. Wang, H. Tang, X. Yan, H. Liu, Catal. Commun. 20 (2012) 29–35.
[78] A. Nowicki, V. Le Boulaire, A. Roucoux, Adv. Synth. Catal. 349 (2007) 2326–2330.
[79] S. Miao, Z. Liu, B. Han, J. Huang, Z. Sun, J. Zhang, T. Jiang, Angew. Chem. Int. Ed. 45 (2006) 266–269.
[80] X. Kang, J. Zhang, W. Shang, T. Wu, P. Zhang, B. Han, Z. Wu, G. Mo, X. Xing, J. Am. Chem. Soc. 136 (2014) 3768–3771.
[81] W.S. Hummers, R.E. Offeman, J. Am. Chem. Soc. 80 (1958) 1339–1339.